Scalable and Environmentally Benign Process for Smart Textile Nanofinishing

Feng, Jicheng; Hontañón, Esther; Blanes, Maria; Meyer, Jörg; Guo, Xiaoai; Santos, Laura; Paltrinieri, Laura; Ramlawi, Nabil; de Smet, L.C.P.M.; Nirschl, Hermann

DOI
10.1021/acsami.6b03632

Publication date
2016

Document Version
Accepted author manuscript

Published in
ACS Applied Materials and Interfaces

Citation (APA)
Feng, J., Hontañón, E., Blanes, M., Meyer, J., Guo, X., Santos, L., Paltrinieri, L., Ramlawi, N., de Smet, L. C. P. M., Nirschl, H., Kruis, F. E., Schmidt-Ott, A., & Biskos, G. (2016). Scalable and Environmentally Benign Process for Smart Textile Nanofinishing. *ACS Applied Materials and Interfaces*, *8*(23), 14756-14765. https://doi.org/10.1021/acsami.6b03632

A Scalable and Environmentally Benign Process for Smart Textile Nanofinishing

Jicheng Feng[1], Esther Hontañón[2], Maria Blanes[3], Jörg Meyer[4], Xiaoai Guo[4], Laura Santos[5], Laura Paltrinieri[1], Nabil Ramlawi[1], Louis de Smet[1], Hermann Nirschl[4], Frank Einar Kruis[2], Andreas Schmidt-Ott[1*]& George Biskos[1, 6, 7*]*

[1]Faculty of Applied Science, Delft University of Technology, Julianalaan 136, 2628 BL, Delft, the Netherlands.

[2]Institute for Technology of Nanostructures and Centre for Nano-integration Duisburg-Essen (CENIDE), University of Duisburg-Essen, Bismarckstr.81, 47057 Duisburg, Germany.

[3]Department of Technical Finishing and Comfort, AITEX, Plaza Emilio Sala 1, 03801 Alcoy, Spain.

[4]Institute for Mechanical Process Engineering and Mechanics, Karlsruhe Institute of Technology (KIT), Strasse am Forum 8, 76131 Karlsruhe, Germany.

[5]Foundation for the Promotion of the Textile Industry (FOMENTEX), Els Telers 20, 46870 Ontinyent, Spain.

[6]Energy Environment and Water Research Center, The Cyprus Institute, Nicosia 2121, Cyprus.

[7]Faculty of Civil Engineering and Geosciences, Delft University of Technology, 2628 CN, Delft, the Netherlands. Correspondence and requests for materials should be addressed to jic.feng@gmail.com; g.biskos@tudelft.nl; a.schmidt-Ott@tudelft.nl

KEYWORDS: nanoparticles, aerosol deposition, textile nanofinishing, antibacterial, leaching test

ABSTRACT

A major challenge in nanotechnology is that of determining how to introduce green and sustainable principles when assembling individual nanoscale elements to create working devices. For instance, textile nanofinishing is restricted by the many constraints of traditional pad-dry-cure processes, such as the use of costly chemical procedures to produce nanoparticles (NPs), the high liquid and energy consumption, the production of harmful liquid waste, and multi-step batch operations. By integrating low-cost, scalable, and environmentally benign aerosol processes of the type proposed here into textile nanofinishing, these constraints can be circumvented while leading to a new class of fabrics. The proposed one-step textile nanofinishing process relies on the diffusional deposition of aerosol NPs onto textile fibers. As proof of this concept, we deposit Ag NPs onto a range of textiles and assess their antimicrobial properties for two strains of bacteria (i.e., *Staphylococcus Aureus* and *Klebsiella Pneumoniae*). The measurements show that the logarithmic reduction in bacterial count reaches ca. 5.5 (corresponding to a reduction efficiency of 99.96%) when the Ag loading is one order of magnitude less (10 ppm; i.e., 10 mg Ag NPs per kg of textile) than in the textiles treated by traditional wet-routes. The antimicrobial activity does not increase in proportion to the Ag content above 10 ppm as a consequence of a “saturation” effect. Such low loading for antimicrobial textiles minimizes the risk to human health (during textile use) and to the ecosystem (after textile disposal), as well as it reduces the changes in color and texture of textile products. After three washes, the release of Ag is in the order of 1wt.%, which is comparable to textiles nanofinished with wet-routes using binders. Interestingly, the washed textiles exhibit almost no reduction in antimicrobial activity, much as those of as-deposited samples. Considering that a realm of functional textiles can be nanofinished with the help of aerosol deposition, our results demonstrate that the proposed approach, which is universal and sustainable, can potentially lead to a wide number of applications.

Introduction

Implementing nanotechnology for manufacturing "smart textiles",[1–4] and developing bioinspired fibers and fabric coatings represent cutting-edge advancements in the field of textile-based products for a wide range of applications. For instance, fabric aesthetics will expand if their optical appearance is manipulated by utilizing plasmonic nanoparticles (NPs).[4,5] In combination with sensor technologies, color-changing fabrics will enable adaptation to surroundings thereby advancing camouflage techniques.[3] What is more, integrating NPs into textiles can also introduce antimicrobial,[6–8] flame retardant,[9,10] self-cleaning,[3] and UV protective properties,[11] while simultaneously helping in the development of wearable devices (e-Textiles),[12–14] and exerting chemical softening effects to the textile fibers. Despite this tremendous range of applications, the dispersion, impregnation, distribution, and immobilization of low NP loads onto textile fibers in a controlled environment remain major challenges, especially when considering the increasing demands for green and sustainable techniques.

Producing functional textiles is currently based on conventional pad-dry-cure processes, which have many shortcomings. These wet-finishing processes rely on chemical reactions in a liquid medium and the use of surfactants. This, in turn, requires reducing agents or templates for the synthesis of colloidal solutions, inevitably resulting in surface contamination on the final nanomaterials.[15] Squeezing out the excess solution from the padded fabric produces liquid waste products, some of which are detrimental to the environment. In addition, if uncontrolled evaporation of the solvent occurs during the drying process, it can cause inhomogeneous distribution of NPs on the fibers due to migration phenomena.[16] This drying procedure also limits the roll-to-roll speed of the

textile finishing line. Another drawback of the wet-finishing process is that the reproducibility and controllability of nanomaterial deposition are frequently inhibited by the batch-type operation.[17] The nanofinished textiles, for instance, can receive high nanomaterial loadings in an uncontrolled fashion with respect to their concentration profile within the textiles. In combination with polymeric binding, which exacerbates fabric texture and comfort, these high loadings raise many concerns in relation to nanomaterial release during washing and disposal.[18,19]

The advancement of textile nanofinishing not only requires implementing a sustainable technology producing complex nanomaterials to enhance performance and to extend the functions of the final product,[1] but also it needs to guarantee financial and environmental viability. Here, we propose a sustainable and universal approach to textile nanofinishing that relies on a single-step NP synthesis and deposition process. Among the various aerosol processes, electrical discharges allow the high-yield synthesis of a wide range of well-defined NPs[20–25] (with respect to NP concentration, size,[26,27] crystallinity,[28] and chemical composition[29,30]) that can be directly deposited onto textile fibers by diffusion, in a green and universal manner. The uniqueness of the proposed process lies in that diffusional deposition can be easily integrated into textile nanofinishing while providing a controlled loading profile within the textiles. In addition to these unique features, the proposed NP synthesis method yields sub-5-nm singlet particles[27,31], whose size can be tuned even down to that of atomic clusters (i.e., of the order of a few Å).[32] Particles in this size range not only provide an extremely large surface area for sufficiently high mass specific activity and diffusional deposition efficiency, but they also guarantee strong adhesion to fibers (given that agglomeration is avoided), thus minimizing their release. Since the NP synthesis method is fully compatible with commercial roll-to-roll textile

production as illustrated in Figure 1, the nanofinishing process proposed here is amenable to upscaling. Although the applications of the proposed method can be numerous, as a proof of the concept we use it here to fabricate antimicrobial textiles and test their activity and washing durability.

Results

Particle size distributions in the gas phase. A scanning mobility particle sizer (SMPS)[33] was used to determine the size distributions of the Ag NPs generated by spark ablation. A tube (with a length of 32 cm and an inner diameter of 4 mm) transfers the aerosol NPs from the depositing point (i.e., the textile sample) to the measuring point (i.e., the SMPS). To account for the coagulational growth of the particles in this sampling tube, theoretical calculations were used to estimate their size distributions when they arrive at the surface of the textile (cf. Section S1 in the Supporting Information). Figure 2a and 2b show lognormal particle size distributions (PSDs) measured by the SMPS (black curves) at two different quenching gas flow rates (Q_q = 20 and 50 standard liters per minute (slm)). The geometric mean diameter (d_p) and the geometric standard deviation (σ_g) of the PSDs of the generated NPs are summarized in Table 1. The size of the particles produced by spark ablation can be easily controlled by varying Q_q.[27] When Q_q increases from 20 to 50 slm, d_p decreases from ca. 3.6 to ca. 1.5 nm, which is corroborated by model predictions.[31] Interestingly, an increase in Q_q does not diminish the deposition efficiency of the NPs significantly (cf. Section S2 in the Supporting Information). As the NP mass production rate is unaffected by the gas flow rate, increasing Q_q only decreases the particle size (i.e., increase the total particle surface area) and therewith the mass specific activity. This observation simplifies the scalability of the proposed textile nanofinishing methodology

with respect to NP synthesis. The size distribution (with d_p = 3.6 nm; cf. Figure 2c) derived from analyzing the TEM image is similar to the estimation based on the SMPS measurements (d_p = 3.9 nm; cf. red curve in Figure 2a). Most of the deposited particles shown in the TEM image (inset in Figure 2c) are non-agglomerated singlet particles. This is highly desirable as singlets have stronger adherence to the fibers than agglomerates, which also simplifies the modeling of NP deposition onto the textile fibers.

Table 1. Mean size d_p and geometric standard deviation σ_g of Ag NPs generated by spark ablation in Ar (purity 99.999%)

Q_q (slm)	d_p (nm)		σ_g	
	SMPS measurements	Deposition on textile[27,31]	SMPS measurements	Deposition on textile[27,31]
20	9.7	3.6	1.53	1.35
50	7.6	1.5	1.48	1.35

Particle deposition on textiles. The deposition efficiency of the particles onto the textile fibers depends on particle size, the textile characteristics, and the flow rate through the fabric. Figure 3 shows all the predicted and measured size-dependent deposition efficiencies of the particles onto different textiles (namely Acrylic-Polyester-Cotton-Polyamide (APCP), Polyester (PES), and Cotton; cf. Table S1 for more details) as a function of particle diameter. Diffusional deposition is the dominant mechanism due to the size of the NPs below 5 nm (cf. Figure 2 and Section S2 in the Supporting Information)[34]. As a result, the deposition efficiency E for any given textile with an averaged solidity α, thickness L, and fiber diameter d_f can be estimated as:[34]

$$E = 1 - \exp\left(\frac{-10.8\alpha L D^{\frac{2}{3}}}{\pi(1-\alpha)d_f^{\frac{5}{3}}U^{\frac{2}{3}}}\right) \quad (1)$$

where $U = Q_q/A$ (A is the deposition area); U is a face velocity, and D is the diffusion coefficient of the particles, which can be determined by equation (S8) given in the Supporting Information. For a fixed U, E depends solely on particle size.

For any given mass production rate and deposition time, equation (1) can be used to estimate the NP loading on the textiles.[27] Predictions by equation (1) are validated with inductively coupled plasma mass spectrometry (ICP-MS) (cf. Table S3). The agreement between measurements and predictions has a practical value, especially when it comes to scaling up the process and building an online system to monitor the NP loading of the treated textile. Another interesting feature is that NP loading decays exponentially as a function of the textile depth (L_d),[35] determined by face velocity during the deposition. As a result, the concentration/loading profile can be tuned (cf. equation (1)) depending on the application.

Observed discrepancies between predictions made by equation (1) and the measurements can be caused by the inhomogeneity of the textiles, which strongly influence the collection efficiency of a filter medium.[36] This is especially true for the Cotton and PES textiles that have impermeable multi-filamentary fibers (i.e., only few fibers extend into the permeable pore structure). APCP textile mainly consists of a 'hairy' tuft of individual fibers (oriented along the upstream side during filtration) which more closely resemble a conventional depth filter structure.

A pressure drop is caused by the combined effect of each fiber resisting the gas flow. Figure 3b shows that the measured pressure drop is linearly dependent on the flow face velocity (cf. Equation (S15)).[34] Since the NP loading does not introduce additional resistance (at least regarding the loading range intended here), the pressure drop for the

raw (without aerosol deposition) and nanofinished textiles (with aerosol deposition) collapses into one single curve as shown in Figure 3b (cf. Table S2).

Surface chemistry and morphology of Ag NPs on textile fibers. The primary particle size, the surface property, and the crystal phase of the Ag NPs are determined by small- and wide-angle X-ray scattering (SAXS/WAXS). The scattering intensity I of the raw and nanofinished Cotton textile was recorded as a function of the scattering angle 2θ or the scattering vector $q = (4\pi \cdot \sin\theta)/\lambda$ (using X-ray (Cu K_α radiation) wavelength λ = 0.154 nm). Figure 4 shows the SAXS/WAXS data for the nanofinished Cotton textile. The scattering intensity follows a power law ($I \propto q^{-4}$) when q ranges from 0.5 to 2 nm^{-1}, which implies that the Ag NPs have a smooth surface with a surface fractal dimension d_s of 2.0. When q is smaller than 0.5 nm^{-1}, the NP radius of gyration R_g was found to be 5.4 nm, which corresponds to a mean diameter d_p of 13.9 nm.[37] This diameter is significantly larger than that estimated by the SMPS measurements (i.e., the red curve in Figure 2b). Such a discrepancy can be attributed to the strong coalescence of high-purity singlets on fibers during deposition.[38] Coalescence ceases when the NPs reach a critical size beyond which agglomerates becomes dominant.[27] Comparing the peaks of the WAXS curves corresponding to the raw fabric with those of the nanofinished fabric, an additional peak at 2θ = 38.1° is related to crystalline phase Ag (111). The acquired signals are relatively weak due to the low NP loading on the fabric (cf. Table S2).

XPS confirms the existence and chemical state of the surface of the three nanofinished textiles. These textiles were examined with XPS on the front side, which was directly facing the aerosol flow during deposition, and the backside, which was in close contact with the textile sample holder. The absence of any additional peaks in the XPS

measurements performed on the backside of the nanofinised textiles as compared to those on the raw textiles indicates the absence of silver at their backside. This is in line with the predictions of equation (1) and the deposition measurements shown in Figure 3a, which indicate that the majority of the particles (depending on their size) are being deposited at the front side of the textiles as the aerosol flows from one side to the other. Consequently, the concentration of the deposited particles decreases with increasing fabric depth. Sub-10-nm particles have 100% deposition efficiency, implying that no Ag particles are present at the backside of the fabric (i.e., all of them are deposited before the flow reaches the backside), as confirmed by the XPS measurements (cf. red curve in Figure 5a).

On the front side, the peaks at 369.7 and 375.7 eV are assigned to the binding energies of Ag $3d_{5/2}$ and Ag $3d_{3/2}$ of metallic Ag^0. The 367.8 and 373.8 eV peaks correspond to the binding energies of Ag $3d_{5/2}$ and Ag $3d_{3/2}$ of Ag^+ (Ag_2O) or to the surface charges of the NPs. A number of studies have reported on the shift of XPS core levels to higher binding energies for sub-10-nm Ag NPs.[39,40] Considering also the (small) difference in the internal standard, the binding energy identified in our measurements suggests that the NPs are smaller than 20 nm in diameter, which is in line with our SMPS results. The chemical state ratio of Ag^+/Ag^0, estimated by the deconvolution of the Ag 3d peaks (cf. Figure 5b), is ca. 3.9 (which is similar to that reported Prieto *et al.*[39]). This is understandable because the surface of Ag NPs undergoes oxidation (also confirmed by the presence of AgMNN peak in the Auger region[41]) when exposed to the atmosphere or to the high-energy electron beam during the XPS measurements. The low amount of NPs deposited in the textiles (cf. Table S3) is responsible for the invisible peak of silver oxides in the WAXS curve (cf. Figure 4b). Note that the positive charges of the Ag NPs could also contribute to Ag^+:

they electrostatically attract the negatively charged bacterial cell membranes thereby promoting antibacterial activity.[18,42]

General macroscopic properties of the nanofinished textiles. The color of the nanofinished textiles depends on the types of fabric (cf. Figures 6 a, e and i) and on the NP loading (Figures 6b, f and j). SEM images with two different magnifications for each textile sample are presented in the last two columns of Figure 6 (c, d, g, h, k, and l). Magnified images show the singlet and agglomerated Ag NPs attached to the surface of the fibers. As shown in Figure 2, the NPs suspended in the gas phase remain non-agglomerated singlets. Particles agglomerate at a later stage after coalescence via collisions with arriving aerosol NPs. Moreover, NP depositions of low loading did not change the woven structure of the fabrics, which indicates that the air-breathing properties that are so vital to textile comfort are preserved.

Antimicrobial properties of the nanofinished textiles. Ag NPs have been widely shown to exhibit antimicrobial activity.[18,43] Although the exact mechanisms of their antimicrobial action is still subject to debate,[44] it is believed that Ag ions released by the NPs interfere with bacterial cell functions upon contact.[43,45–49] The Ag ions penetrate the bacterial cell wall, and subsequently bind DNA molecules, leading to a loss of the ability to replicate. At the same time, Ag NPs inactivate and denaturate proteins because they tend to have a greater capacity to react with sulphur-containing proteins and phosphorous-containing DNA. These phenomena lead to the degradation or death of the microorganisms.[46,47] Electrostatic attraction between bacterial cells and particles can also have an impact on antibacterial activity (AA),[47–49] whereas reactive oxygen species can damage lipids, proteins, and the DNA of microorganisms.[45]

The AA of the nanofinished textiles was assessed in accordance with the International Standard ISO20743 (quantitative method). All the nanofinished textiles assessed in this work exhibit strong AA (>3). An AA of ca. 5 is equivalent to a colony forming unit (CFU) reduction efficiency of 99.96% (see Methods). The high AA values shown in Figure 7a can be attributed to the large specific surface area and to the associated fast ion release rate of the NPs that were synthesized and used here.[43] In contrast to traditional wet-finishing processes,[18,50,51] the textiles with such low Ag NP loading (in the order of 10 ppm) still have high antimicrobial efficiency (against *Staphylococcus Aureus* (SA) and *Klebsiella Pneumoniae* (KP), as shown respectively in the left and right columns in Figure 7a). Minor differences in AA against SA and KP can be explained by the dissimilar defense systems of the two species against Ag ions[46]. Viability assays show no statistically significant change in the AA of the textiles with concentrations above ca. 15 ppm. Changes above this limit cannot be determined by standard method employed to test the AA (cf. Methods), due to 'saturation' of the method.[44] This means that by exceeding a NP loading level, the CFU reduction efficiency remains roughly 100% (more specifically, 99.96% for AA of 5).

The AA values of the different nanofinished textiles after washing are presented in Figure 7b. Interestingly, the AA remains as high as 5.5 after three washing cycles. The decreased AA of nanofinished LYS (from 5.6 to 4.2; Lyocell Safari in Table S1) is attributed to its lower Ag content (12 ppm) which is not sufficient to reach the AA saturation point. Although this Ag content is ca. 50 times lower than that reported in previous work[50], a high AA is still retained.[52] The comparatively low Ag content required to achieve high AA values when dry deposition is used, may be attributed to the homogenous NP

coverage, their size which is in the sub-10-nm range, and the faster ion release. In contrast to the results reported by Hebeish *et al*.,[53] the AA of LYZ (Lyocell Zen in Table S1) textile is higher in the washed rather than in the unwashed samples. A possible reason for this is that the pH of the detergent used for washing considerably promotes Ag ion release.[43] On the other hand, compounds (e.g., starch, protein derivatives, fats and oils) typically used on the textiles that serve as nutrients for the bacteria are easily washed away, thereby resulting in an increased AA after washing.

Washing durability of the nanofinished textiles. In connection with the release of Ag NPs from textiles, the laundering durability is of paramount importance to their reuse. To determine that, we carried out a mechanical washing test following the standard method (ISO 105-C06:2010). Figure 8a shows that a high NP release was observed for the first washing cycle (ca. 5-33%). Less Ag was released in the second wash (< 5 %) gradually decreasing to ca. 1 wt.% after three washing cycles (one order of magnitude lower than that seen in commercial fabrics[51]), indicating good washing durability. We ascribe the higher release of Ag in the first wash to the agglomerates formed in the first layers of the fabric facing the aerosol flow (cf. Figure S4). Such agglomerates easily become detached from the fibers during washing.[51] Even after three washing cycles, virtually no decay is observed in the AA of the nanofinished textiles, implying that a lower amount of Ag NPs (ca. 10 ppm) would be sufficient to achieve an AA value of ca. 5. To reduce the release of Ag while still retaining high AA, the nanofinished textiles can therefore be appropriately washed before use.

Lower NP loading can prevent the formation of agglomerates on the fibers while maintaining high AA, as demonstrated by Lok *et al*.[54] Particle size distribution

measurements (cf. Figure 2) confirm that the NPs remain non-agglomerated singlets when suspended in the gas.[27] The deposition of such singlets should decrease particle release in conjunction with strong particle adhesion to the fibers when compared to larger particles or agglomerates. Both enhanced adhesion and a large exposed surface can thus be achieved by making the particles small.[54] Deposition of NPs deeper within the textiles, which should also reduce their release during mechanical washing, can be achieved by simply increasing the quenching gas flow rate Q_q as indicated by equation (1) (cf. Figure S5). The size of the resulting Ag NPs also reduces to the sub-5-nm, which helps in realizing a minimum deposition level. Ultimately, this low NP loading can reduce the potential environmental and human health impacts while guaranteeing the comfort of textiles as their texture will remain unchanged.[55] Apart from the influence of particle size on the release, the type of textiles also plays a role as indicated by the leaching test shown in Figure 8a. In addition, the formation of agglomerates on the front layers of the fabric, due to the longer deposition as discussed above, contributes substantially not only to the high Ag content but also to the imminent release in the mechanical washing process (cf. Figure 8b).

Discussion

In this work, we have combined, for the first time, NP synthesis in the gas phase with diffusional deposition to realize a novel pathway for the next generation of multifunctional textiles. Put briefly: sub-10-nm NPs carried by a gas flow are passed through the fabric, where they rapidly diffuse and attach to the textile fibers. This approach does not require any stabilization steps or reducing agents, does not produce any effluents, and has small energy consumption, thereby gaining financial and environmental benefits. In addition, the fast kinetics of NP formation in the

gas phase represents a dramatic increase in the process throughput, which addresses one of the bottlenecks seen in large-scale textile nanofinishing.

As proof of this concept, among the numerous potential applications of the functionalized textiles, we show that the antimicrobial activity of a number of textiles nanofinished with Ag NPs is high. Although the NP loads used here were one order of magnitude lower than those used in traditional wet-finishing routes, they were shown to be sufficient for achieving high antibacterial activity even after three wash cycles. The antimicrobial textiles outperform those reported in the literature due to the particle size which lies in the sub-10-nm range, the good mechanical durability, the absence of liquid precursors, the desired finishing surface, the easy scalability, and the virtually unlimited mixing combinations of NPs.

Investigating the size-effect of the NPs can also provide an opportunity to improve fundamental understanding of particle-cell interactions, which have been impossible to investigate up until now. Despite the small NP loadings (even in the order of 10 ppm), compared to those used in other studies, the plateau ("saturation effect") in the antimicrobial activity of the nanofinished fabrics reported here can be attributed to the size and the composition of the particles employed. To reveal the NP size-dependent effects in future work, one will have to use even smaller loadings and also avoid the formation of agglomerates on the fibers, thus minimizing their release due to the strong adhesion of the singlets to the fibers. The low loading of NPs on textiles can also maintain conformal contact with the human body in a non-invasive way.

When agglomerates cannot be avoided, to improve the washing durability of the nanofinised fabrics, one can bind them to the textile fibers by introducing covalent linkage (e.g., thiol group) to textile fibers.[45,56] Surface area of the agglomerates is

approximately equal to the sum of individual particles, thus providing comparable antimicrobial properties. Note that here we do not fabricate NP surface. The reason for this is to maintain the simplicity of the NP production method. Another reason is that the non-fabricated NPs tend to further agglomerate when released in an aquatic environment. These large agglomerates are no longer able to cross biological barriers, such as the blood-brain or placenta barrier.[55] The risks are consequently eradicated as compared to those linked to using surfactants to prevent further agglomeration.[55]

Nanofinished textiles can release a fraction of the deposited NPs upon washing, and thus reduce their antimicrobial activity and have an impact on the environment.[57] Although the NP release mechanism can vary depending on the temperature and the pH of the deterrent,[58–61] we used the standard ISO 105-C06:2010 washing method at the most harsh conditions,[62] which fixed a pH of 6.5~7.0 and temperature at 90 ^{o}C. Doing so facilitates comparison with other studies[51] and maintains textile properties (e.g., color, comfort, and texture) for long-term use.

Despite the tremendous global market of smart textiles,[4] the major concern lies in their potential release of the NPs to the environment.[57] Ag NPs, or ions released from their surfaces, that end up to the wastewater can inhibit the growth of bacteria in treatment plants and/or become toxic to aquatic life.[63] Future life cycle evaluations should also take into account the type of nanomaterials, their solubility, and oxidizing capacity.

Conclusion

We have presented here a universal and sustainable way for one-step textile nanofinishing by incorporating aerosol NP production and deposition onto fibers. This enables the proposed approach to stand out from all the multi-step finishing processes employed so far. As proof of the

concept, we have studied the antibacterial activity (AA) of a number of textiles loaded with Ag NPs at concentrations in the order of 10 ppm. These textiles exhibited AA of ca. 5.5 (logarithmic reduction in bacterial count) which corresponds to a colony forming unit (CFU) reduction efficiency of ca. 99.96%. This high AA is maintained even after three washing cycles. Although Ag release by mechanical washing is one order of magnitude lower than that of commercial nanofinished textiles, the washing durability can still be enhanced by introducing covalent linkage between Ag NPs and thiol-modified cellulose fibers. The proposed approach also allows tuning the depth profile and the size of the NPs deposited in textiles, which lies beyond the capabilities of pad-dry-cure processes and can be used to further improve the washing durability. Although this study demonstrates the antimicrobial properties of the treated textiles with Ag NPs, the concept can be extended to diverse material combinations for the preparation of multifunctional textiles. Since the performance of nanofinished textiles still needs to be further investigated and improved, concerted effort is still required to understand the impact that released nanomaterials can have on humans and ecosystems.

Methods

Nanoparticle synthesis. Electrical discharges were used to produce Ag NPs, namely spark ablation[64], and arc discharge.[65] With the former method, a spark discharge is initiated by a self-pulsed circuit operating in parallel with a capacitor bank and with two electrodes (two identical 99.99% pure Ag rods with a diameter of 3 mm and a length of 30 mm, MaTecK GmbH, Germany) placed next to each other forming a gap through which the carrier gas (Ar purity 99.999%) flushes through. The electrodes in the arc discharge are a tungsten rod (with a diameter of 1.6 mm, purity 99.95%, Goodfellow Cambridge Ltd., UK), and an Ag rod (with a diameter of 9.5 mm, purity 99.9%, Goodfellow GmbH, Germany) using the carrier gas of N_2 (purity 99.999%). In these methods, the Ag electrode evaporates due to the energy delivered by the discharge. The vapors are quenched by the carrier gas, thereby leading to the formation of NPs through homogeneous nucleation, and subsequent condensation.

Size distributions of the particles. A scanning mobility particle sizer (SMPS) was used to measure the size distribution of the particles.[33] The system consists of a differential mobility analyzer (DMA), and a Faraday cup aerosol electrometer (AEM). The DMA selects particles based on their electrical mobility, whereas the AEM counts the numbers of the charged monodisperse particles downstream of the DMA.

Textile Nanofinishing by means of the aerosol deposition. The textile performance was evaluated by measuring the filtration efficiency and the pressure drop. The aerosol flow passes through the textile, with the textile acting as a filter. The textiles (Cotton, PES, and APCP) consisted of a mat of fine fibers arranged perpendicularly to the aerosol flow direction and with a fiber diameter of ca. 20 µm. The face velocity ranged from 0.5 to 4 cm s^{-1}. Because the aerosol NPs are sub-10-nm, their Brownian motion guarantees the collision with the fiber while flowing around in a non-intercepting streamline, whereas upon collision van der Waals forces that ensure that NPs stick to the fibers.

Filtration properties of the textiles. To investigate the filtration efficiency of NPs (sintered, size-classified Ag spheres) for different textiles, their concentrations at the inlet and outlet of the textile holder were measured using two condensation particle counters (CPC Model 3775, TSI). The filtration efficiency results were calibrated for particle losses in the tubing and textile holder as well as for differences in the counting

efficiencies of the each CPC, based on reference measurements when there were no textile samples in the holder. The filter pressure drop Δp at various face velocities (0.5, 1, 2, 4 cm s^{-1}) was measured using a sensitive handheld differential pressure transducer (Model 521-3, Testo) connected to the upstream and downstream ports of the textile holder. Δp across the filter was obtained by subtracting the measured pressure drop across the empty textile holder from the measured pressure drop across the entire holder and textile assembly. Details of the setup are shown in the Figure S3.

Analysis of the Ag content of the fabrics by means of ICP-MS. Three replicates of 0.2 ± 0.04 g from each textile were digested with 3 ml HNO_3 (65%, Fluka) and 1.5 ml HCl (95%, Sigma–Aldrich), and were attained in a microwave digestion system (ULTRAWAY of MILESTONES). The Ag content of the digests was quantified by means of inductively coupled plasma mass spectroscopy (ICP-MS Perkin-Elmer OPTIMA 7700), which was calibrated with a silver standard solution ($AgNO_3$ in 5 M HNO_3, 1000 mg L^{-1}, Merck).

Antimicrobial activity of the nanofinished textiles. The antibacterial activity of the fabrics was tested according to a standard method (ISO 20743: 2013) using the Gram-negative bacterium *Klebsiella pneumonia* ATCC 4352 (LMG 3128) and the Gram-positive bacterium *Staphylococcus Aureus* ATCC 6538 (CECT 239). All textiles used in this work were placed into 0.2-mL of inoculum ($1\sim3\times10^5$ CFU mL^{-1}) and 20 mL of neutralizing agent per 0.4 g of fabric. This standard always made use of a reference fabric (C values). The antimicrobial activity (AA) was determined by counting the number of bacterial colonies and was calculated according to the logarithm reduction of CFU given by:

$$\mathrm{AA} = \log\left(\frac{C_t/C_0}{T_t/T_0}\right) \qquad (2)$$

where C_0 and C_t are the CFU of control/untreated samples at times 0 and 18 h; T_0 and T_t are the CFU of test/treated (or nanofinished) samples at times 0 h and 18 h. In the standard method employed in the antimicrobial activity, the CFU below 2000 is always considered. Changes exceeding this limit cannot be determined in the standard method. In order to obtain an averaged AA, the tests were repeated three times. Each measurement used two control samples (raw fabric) for reference purposes and two test samples (treated fabrics). According to Annex F of ISO 20743: 2013, the antibacterial property of the test fabric can be considered as "significant" when $2 \leq AA < 3$ and "strong" when $AA \geq 3$.

Washing durability of the nanofinished textiles. The washing procedure was conducted according to a standard method (ISO 105-C06:2010). A washing machine (ATLAS Linitest) equipped with steel vessels that had a capacity of 550 ml and a motor speed of 40 ± 2 rpm was used for all the tests. Ten steel balls previously cleaned in HNO_3 (65%) were used to exert mechanical stress. It was ensured that the detergent/container volume ratio (0.279) was the same as that in the steel vessel. The detergent was prepared by dispersing 4g L^{-1} ECE 98-standard washing powder in distilled water (composition: 9.7% LAS, 5.2% non-ionic surfactant, 3.6% soap, 4.5% antifoam, 32.5% zeolite, 11.8% carbonate, 5.2% acrylic acid, 3.4% Na-silicate, 1.3% CMC, 0.8% phosphonate, 9.8% sulphate, 12.2% others/water)[60]. The textiles (2 samples; 40×100 mm^2) were washed for 55 min at 90 ºC. Acid-cleaned polyethylene bottles (100 ml) were used to recover the detergent from the washing machine. The detergent was analysed by means of ICP-MS to determine the Ag content embedded in the textiles (mg/kg). We performed three cycles for each nanofinished textile sample.

Surface chemistry and morphology of the nanofinished textiles. A transmission electron microscopy (TEM, Philips CM30T and Philips CM12) and a scanning electron microscopy (SEM, Hitachi S-3400N and Hitachi S-4500) were used to image the particles in order to determine their size, structure and morphology. For the TEM measurement, an MPS was used to collect the particles on the TEM grids (Van Loenen Instruments, S143-3 Q'foil 1.2/1.3 400 Cu) by means of filtration.[66]

Detailed information on the structure of the particles found on the fibers were obtained by small- and wide-angle X-ray scattering (SAXS/WAXS). Non-invasive measurements were performed using a custom-made laboratory SAXS/WAXS camera with Cu-Kα radiation (λ = 1.54 Å), as described elsewhere.[67] To obtain sufficiently accurate statistical results, each sample with an area of ca. 0.5 × 1.5 cm^2 was positioned inside the SAXS/WAXS measuring chamber and illuminated by the incident X-ray beam. The scattering signals were simultaneously recorded within a detection angle of 90°.

X-ray Photoelectron Spectrometer (Thermo Fisher Scientific Kα model) examination was carried out for the elemental analysis of the nanofinished textiles. A monochromatic Al Kα X-ray source was used which had a spot size of 200 μm at a pressure of 10^{-8} mbar and a constant pass energy of 10 eV; the flood gun was turned on during the measurements in order to compensate the potential charging of the surface. The peak

positions in the narrow scan spectra were adjusted according to the internal standard C1s peak at 284.5 eV, with an accuracy of ± 0.05 eV.

Supporting Information. The calculation of particle size distribution at the location of textiles, modeling the deposition of NPs onto textiles, the measurements of filtration efficiency and pressure drop of the textiles, the determination of Ag content on textiles, the schematic illustration of experimental setup. This material is available free of charge via the Internet at http://pubs.acs.org.

Corresponding Authors

Jic.feng@gmail.com; g.biskos@tudelft.nl; a.schmidt-ott@tudelft.nl

Author contributions

The manuscript was written through contributions of all authors. All authors have given approval to the final version of the manuscript.

Funding Sources

the European Union's Seventh Framework Program (EU FP7)

Acknowledgment

This work has been funded by the European Union's Seventh Framework Program (EU FP7) under Grant Agreement No. 280765 (BUONAPART-E). The authors are grateful to Drs. Diane Butterman-Dorey for the proofreading and to Dr. Anne Maisser for the discussions. We would also like to thank Joost Middelkoop, Tobias V. Pfeiffer, Linus Ludvigsson, and Maria E Messing for the TEM and SEM measurements.

REFERENCES

(1) Service, R. F. Technology. Electronic Textiles Charge Ahead. *Science (80-.).* **2003**, *301* (5635), 909–911.

(2) Hamedi, M.; Forchheimer, R.; Inganäs, O. Towards Woven Logic from Organic Electronic Fibres. *Nat. Mater.* **2007**, *6* (5), 357–362.

(3) Dolgin, E. Textiles: Fabrics of Life. *Nature* **2015**, *519* (7544), S10–S11.

(4) Yetisen, A. K.; Qu, H.; Manbachi, A.; Butt, H.; Dokmeci, M. R.; Hinestroza, J. P.; Skorobogatiy, M.; Khademhosseini, A.; Yun, S. H. Nanotechnology in Textiles. *ACS Nano* **2016**, *10* (3), 3042–3068.

(5) Hinestroza, J. P. Can Nanotechnology Be Fashionable? *Mater. Today* **2007**, *10* (9), 56.

(6) Dickerson, M. B.; Sierra, A. A.; Bedford, N. M.; Lyon, W. J.; Gruner, W. E.; Mirau, P. A.; Naik, R. R. Keratin-Based Antimicrobial Textiles, Films, and Nanofibers. *J. Mater. Chem. B* **2013**, *1* (40), 5505.

(7) Zille, A.; Fernandes, M. M.; Francesko, A.; Tzanov, T.; Fernandes, M.; Oliveira, F. R.; Almeida, L.; Amorim, T.; Carneiro, N.; Esteves, M. F.; Souto, A. P. Size and Aging Effects on Antimicrobial Efficiency of Silver Nanoparticles Coated on Polyamide Fabrics Activated by Atmospheric DBD Plasma. *ACS Appl. Mater. Interfaces* **2015**, *7* (25), 13731–13744.

(8) Deng, X.; Yu Nikiforov, A.; Coenye, T.; Cools, P.; Aziz, G.; Morent, R.; De Geyter, N.; Leys, C. Antimicrobial Nano-Silver Non-Woven Polyethylene Terephthalate Fabric via an Atmospheric Pressure Plasma Deposition Process. *Sci. Rep.* **2015**, *5* (May), 10138.

(9) Mayer-Gall, T.; Knittel, D.; Gutmann, J. S.; Opwis, K. Permanent Flame Retardant Finishing of Textiles by Allyl-Functionalized Polyphosphazenes. *ACS Appl. Mater. Interfaces* **2015**, *7* (18), 9349–9363.

(10) Chen, S.; Li, X.; Li, Y.; Sun, J. Intumescent Flame-Retardant and Self-Healing Superhydrophobic Coatings on Cotton Fabric. *ACS Nano* **2015**, *9* (4), 4070–4076.

(11) Xiao, X.; Liu, X.; Chen, F.; Fang, D.; Zhang, C.; Xia, L.; Xu, W. Highly Anti-UV Properties of Silk Fiber with Uniform and Conformal Nanoscale TiO2 Coatings via Atomic Layer Deposition. *ACS Appl. Mater. Interfaces* **2015**, *7* (38), 21326–21333.

(12) Liu, L.; Yu, Y.; Yan, C.; Li, K.; Zheng, Z. Wearable Energy-Dense and Power-Dense Supercapacitor Yarns Enabled by Scalable Graphene–metallic Textile Composite Electrodes. *Nat. Commun.* **2015**, *6*, 7260.

(13) Stoppa, M.; Chiolerio, A. Wearable Electronics and Smart Textiles: A Critical Review. *Sensors* **2014**, *14* (7), 11957–11992.

(14) Hu, L.; Pasta, M.; Mantia, F. La; Cui, L.; Jeong, S.; Deshazer, H. D.; Choi, J. W.; Han, S. M.; Cui, Y. Stretchable, Porous, and Conductive Energy Textiles. *Nano Lett.* **2010**, *10* (2), 708–714.

(15) Verma, A.; Stellacci, F. Effect of Surface Properties on Nanoparticle-Cell Interactions. *Small* **2010**, *6* (1), 12–21.

(16) Von Goetz, N.; Lorenz, C.; Windler, L.; Nowack, B.; Heuberger, M.; Hungerbühler, K. Migration of Ag- and TiO2-(Nano)particles from Textiles into Artificial Sweat under Physical Stress: Experiments and Exposure Modeling. *Environ. Sci. Technol.* **2013**, *47* (17), 9979–9987.

(17) Sebastian, V.; Arruebo, M.; Santamaria, J. Reaction Engineering Strategies for the Production of Inorganic Nanomaterials. *Small* **2014**, *10* (5), 835–853.

(18) Richter, A. P.; Brown, J. S.; Bharti, B.; Wang, A.; Gangwal, S.; Houck, K.; Cohen Hubal, E. a.; Paunov, V. N.; Stoyanov, S. D.; Velev, O. D. An Environmentally Benign Antimicrobial Nanoparticle Based on a Silver-Infused Lignin Core. *Nat. Nanotechnol.* **2015**, *10*, 817–823.

(19) Walser, T.; Limbach, L. K.; Brogioli, R.; Erismann, E.; Flamigni, L.; Hattendorf, B.; Juchli, M.; Krumeich, F.; Ludwig, C.; Prikopsky, K.; Rossier, M.; Saner, D.; Sigg, A.; Hellweg, S.; Günther, D.; Stark, W. J. Persistence of Engineered Nanoparticles in a Municipal Solid-Waste Incineration Plant. *Nat. Nanotechnol.* **2012**, *7* (8), 520–524.

(20) Anastasopol, A.; Pfeiffer, T. V; Middelkoop, J.; Lafont, U.; Canales-Perez, R. J.; Schmidt-Ott, A.; Mulder, F. M.; Eijt, S. W. H. Reduced Enthalpy of Metal Hydride Formation for Mg-Ti Nanocomposites Produced by Spark Discharge Generation. *J. Am. Chem. Soc.* **2013**, *135* (21), 7891–7900.

(21) Han, K.; Kim, W.; Yu, J.; Lee, J.; Lee, H.; Gyu Woo, C.; Choi, M. A Study of Pin-to-Plate Type Spark Discharge Generator for Producing Unagglomerated Nanoaerosols. *J. Aerosol Sci.* **2012**, *52*, 80–88.

(22) Boissiere, C.; Grosso, D.; Chaumonnot, A.; Nicole, L.; Sanchez, C. Aerosol Route to Functional Nanostructured Inorganic and Hybrid Porous Materials. *Adv. Mater.* **2011**, *23* (5), 599–623.

(23) Byeon, J. H.; Kim, J.-W. Ambient Plasma Synthesis of TiO2@graphite Oxide Nanocomposites for Efficient Photocatalytic Hydrogenation. *J. Mater. Chem. A* **2014**, *2* (19), 6939–6944.

(24) Byeon, J. H.; Park, J. H.; Yoon, K. Y.; Hwang, J. Ambient Spark Generation to Synthesize Carbon-Encapsulated Metal Nanoparticles in Continuous Aerosol Manner. *Nanoscale* **2009**, *1* (3), 339–343.

(25) Heurlin, M.; Magnusson, M. H.; Lindgren, D.; Ek, M.; Wallenberg, L. R.; Deppert, K.; Samuelson, L. Continuous Gas-Phase Synthesis of Nanowires with Tunable Properties. *Nature* **2012**, *492* (7427), 90–94.

(26) Sengar, S. K.; Mehta, B. R.; Kumar, R.; Singh, V. In-Flight Gas Phase Growth of Metal/multi Layer Graphene Core Shell Nanoparticles with Controllable Sizes. *Sci. Rep.* **2013**, *3*, 2814.

(27) Feng, J.; Biskos, G.; Schmidt-Ott, A. Toward Industrial Scale Synthesis of Ultrapure Singlet Nanoparticles with Controllable Sizes in a Continuous Gas-Phase Process. *Sci. Rep.* **2015**, *5*, 15788.

(28) Grammatikopoulos, P.; Cassidy, C.; Singh, V.; Sowwan, M. Coalescence-Induced Crystallisation Wave in Pd Nanoparticles. *Sci. Rep.* **2014**, *4*, 5779.

(29) Byeon, J. H.; Park, J. H.; Hwang, J. Spark Generation of Monometallic and Bimetallic Aerosol Nanoparticles. *J. Aerosol Sci.* **2008**, *39* (10), 888–896.

(30) Byeon, J. H.; Kim, J.-W. Fabrication of Bimetallic Nanostructures via Aerosol-Assisted Electroless Silver Deposition for Catalytic CO Conversion. *ACS Appl. Mater. Interfaces* **2014**, *6* (5), 3105–3110.

(31) Feng, J.; Huang, L.; Ludvigsson, L.; Messing, M. E.; Maisser, A.; Biskos, G.; Schmidt-Ott, A. General Approach to the Evolution of Singlet Nanoparticles from a Rapidly Quenched Point Source. *J. Phys. Chem. C* **2016**, *120* (1), 621–630.

(32) Tyo, E. C.; Vajda, S. Catalysis by Clusters with Precise Numbers of Atoms. *Nat. Nanotechnol.* **2015**, *10* (7), 577–588.

(33) Wang, S. C.; Flagan, R. C. Scanning Electrical Mobility Spectrometer. *Aerosol Sci. Technol.* **1990**, *13* (2), 230–240.

(34) Hinds, W. C. *Aerosol Technology: Properties, Behavior, and Measurement of Airborne Particles*; John Wiley & Sons: New York, 1999.

(35) Thomas, D.; Penicot, P.; Contal, P.; Leclerc, D.; Vendel, J. Clogging of Fibrous Filters by Solid Aerosol Particles Experimental and Modelling Study. *Chem. Eng. Sci.* **2001**, *56* (11), 3549–3561.

(36) Schweers, E.; Löffler, F. Realistic Modelling of the Behaviour of Fibrous Filters through Consideration of Filter Structure. *Powder Technol.* **1994**, *80* (3), 191–206.

(37) Beaucage, G. Approximations Leading to a Unified Exponential/Power-Law Approach to Small-Angle Scattering. *J. Appl. Crystallogr.* **1995**, *28* (6), 717–728.

(38) Sun, J.; He, L.; Lo, Y.-C.; Xu, T.; Bi, H.; Sun, L.; Zhang, Z.; Mao, S. X.; Li, J. Liquid-like Pseudoelasticity of Sub-10-Nm Crystalline Silver Particles. *Nat. Mater.* **2014**, *13* (October), 1007–1012.

(39) Prieto, P.; Nistor, V.; Nouneh, K.; Oyama, M.; Abd-Lefdil, M.; Díaz, R. XPS Study of Silver, Nickel and Bimetallic Silver–nickel Nanoparticles Prepared by Seed-Mediated Growth. *Appl. Surf. Sci.* **2012**, *258* (22), 8807–8813.

(40) Lopez-Salido, I.; Lim, D. C.; Kim, Y. D. Ag Nanoparticles on Highly Ordered Pyrolytic Graphite (HOPG) Surfaces Studied Using STM and XPS. *Surf. Sci.* **2005**, *588* (1-3), 6–18.

(41) Scandurra, A.; Indelli, G. F.; Spartà, N. G.; Galliano, F.; Ravesi, S.; Pignataro, S. Low-Temperature Sintered Conductive Silver Patterns Obtained by Inkjet Printing for Plastic Electronics. *Surf. Interface Anal.* **2010**, *42* (6-7), 1163–1167.

(42) Levard, C.; Hotze, E. M.; Lowry, G. V; Brown, G. E. Environmental Transformations of Silver Nanoparticles: Impact on Stability and Toxicity. *Environ. Sci. Technol.* **2012**, *46* (13), 6900–6914.

(43) Xiu, Z.; Zhang, Q.; Puppala, H. L.; Colvin, V. L.; Alvarez, P. J. J. Negligible Particle-Specific Antibacterial Activity of Silver Nanoparticles. *Nano Lett.* **2012**, *12*, 4271–4275.

(44) Morones, J. R.; Elechiguerra, J. L.; Camacho, A.; Holt, K.; Kouri, J. B.; Ramírez, J. T.; Yacaman, M. J. The Bactericidal Effect of Silver Nanoparticles. *Nanotechnology* **2005**, *16* (10), 2346–2353.

(45) Simon i, B.; Klemen i, D. Preparation and Performance of Silver as an Antimicrobial Agent for Textiles: A Review. *Text. Res. J.* **2016**, *86* (2), 210–223.

(46) Feng, Q. L.; Wu, J.; Chen, G. Q.; Cui, F. Z.; Kim, T. N.; Kim, J. O. A Mechanistic Study of the Antibacterial Effect of Silver Ions on Escherichia Coli and Staphylococcus Aureus. *J. Biomed. Mater. Res.* **2000**, *52* (4), 662–668.

(47) Sondi, I.; Salopek-Sondi, B. Silver Nanoparticles as Antimicrobial Agent: A Case Study on E. Coli as a Model for Gram-Negative Bacteria. *J. Colloid Interface Sci.* **2004**, *275* (1), 177–182.

(48) Stoimenov, P. K.; Klinger, R. L.; Marchin, G. L.; Klabunde, K. J. Metal Oxide Nanoparticles as Bactericidal Agents.pdf. *Langmuir* **2002**, *18* (17), 6679–6686.

(49) Kim, J. S.; Kuk, E.; Yu, K. N.; Kim, J.-H.; Park, S. J.; Lee, H. J.; Kim, S. H.; Park, Y. K.; Park, Y. H.; Hwang, C.-Y.; Kim, Y.-K.; Lee, Y.-S.; Jeong, D. H.; Cho, M.-H. Antimicrobial Effects of Silver Nanoparticles. *Nanomedicine* **2007**, *3* (1), 95–101.

(50) Thanh, N. V. K.; Phong, N. T. P. Investigation of Antibacterial Activity of Cotton Fabric Incorporating Nano Silver Colloid. *J. Phys. Conf. Ser.* **2009**, *187*, 1–7.

(51) Lorenz, C.; Windler, L.; von Goetz, N.; Lehmann, R. P.; Schuppler, M.; Hungerbühler, K.; Heuberger, M.; Nowack, B. Characterization of Silver Release from Commercially Available Functional (nano)textiles. *Chemosphere* **2012**, *89* (7), 817–824.

(52) Gavanji, S. The Effects of Silver Nano Particles on Microorganisms : A Review. *Appl. Sci. Reports* **2013**, *1* (2), 50–56.

(53) Hebeish, A. Green Synthesis of Silver Nanoparticles and Their Application to Cotton Fabrics. *Int. J. Biol. Macromol.* **2015**, *72*, 1384–1390.

(54) Lok, C.-N.; Ho, C.-M.; Chen, R.; He, Q.-Y.; Yu, W.-Y.; Sun, H.; Tam, P. K.-H.; Chiu, J.-F.; Che, C.-M. Silver Nanoparticles: Partial Oxidation and Antibacterial Activities. *J. Biol. Inorg. Chem.* **2007**, *12* (4), 527–534.

(55) Som, C.; Wick, P.; Krug, H.; Nowack, B. Environmental and Health Effects of Nanomaterials in Nanotextiles and Façade Coatings. *Environ. Int.* **2011**, *37* (6), 1131–1142.

(56) Deng, X.; Yu Nikiforov, A.; Coenye, T.; Cools, P.; Aziz, G.; Morent, R.; De Geyter, N.; Leys, C. Antimicrobial Nano-Silver Non-Woven Polyethylene Terephthalate Fabric via an Atmospheric Pressure Plasma Deposition Process. *Sci. Rep.* **2015**, *5*, 10138.

(57) Reed, R. B.; Zaikova, T.; Barber, A.; Simonich, M.; Lankone, R.; Marco, M.; Hristovski, K.; Herckes, P.; Passantino, L.; Fairbrother, D. H.; Tanguay, R.; Ranville, J. F.; Hutchison, J. E.; Westerhoff, P. K. Potential Environmental Impacts and Antimicrobial Efficacy of Silver- and Nanosilver-Containing Textiles. *Environ. Sci. Technol.* **2016**, *50* (7), 4018–4026.

(58) Kulthong, K.; Srisung, S.; Boonpavanitchakul, K.; Kangwansupamonkon, W.; Maniratanachote, R. Determination of Silver Nanoparticle Release from Antibacterial Fabrics into Artificial Sweat. *Part. Fibre Toxicol.* **2010**, *7* (8), 1–9.

(59) Stefaniak, A. B.; Duling, M. G.; Lawrence, R. B.; Thomas, T. a.; LeBouf, R. F.; Wade, E. E.; Abbas Virji, M. Dermal Exposure Potential from Textiles That Contain Silver Nanoparticles. *Int. J. Occup. Environ. Health* **2014**, *20* (3), 220–234.

(60) Geranio, L.; Heuberger, M.; Nowack, B. The Behavior of Silver Nanotextiles during Washing. *Environ. Sci. Technol.* **2009**, *43* (21), 8113–8118.

(61) Pohle, D.; Damm, C.; Neuhof, J.; Rosch, A.; Munstedt, H. Antimicrobial Properties of Orthopaedic Textiles after in-Situ Deposition of Silver Nanoparticles. *Polym. Polym. Compos.* **2007**, *15* (5), 357–363.

(62) Mitrano, D. M.; Rimmele, E.; Wichser, A.; Erni, R.; Height, M.; Nowack, B. Presence of Nanoparticles in Wash Water from Conventional Silver and Nano-Silver Textiles. *ACS Nano* **2014**, *8* (7), 7208–7219.

(63) Bianco, C.; Kezic, S.; Crosera, M.; Svetličić, V.; Šegota, S.; Maina, G.; Romano, C.; Larese, F.; Adami, G. In Vitro Percutaneous Penetration and Characterization of Silver from Silver-Containing Textiles. *Int. J. Nanomedicine* **2015**, *10* (1), 1899–1908.

(64) Schwyn, S.; Garwin, E.; Schmidt-Ott, A. Aerosol Generation by Spark Discharge. *J. Aerosol Sci.* **1988**, *19* (5), 639–642.

(65) Hontañón, E.; Palomares, J. M.; Stein, M.; Guo, X.; Engeln, R.; Nirschl, H.; Kruis, F. E. The Transition from Spark to Arc Discharge and Its Implications with Respect to Nanoparticle Production. *J. Nanoparticle Res.* **2013**, *15* (9), 1957.

(66) R'mili, B.; Le Bihan, O. L. C.; Dutouquet, C.; Aguerre-Charriol, O.; Frejafon, E. Particle Sampling by TEM Grid Filtration. *Aerosol Sci. Technol.* **2013**, *47* (7), 767–775.

(67) Guo, X.; Wagner, M.; Gutsche, A.; Meyer, J.; Seipenbusch, M.; Nirschl, H. Laboratory SWAXS Combined with a Low-Pressure Impactor for Quasi-Online Analysis of Nanoparticles Generated by Spark Discharge. *J. Aerosol Sci.* **2015**, *85*, 17–29.

Figure and Figure Captions:

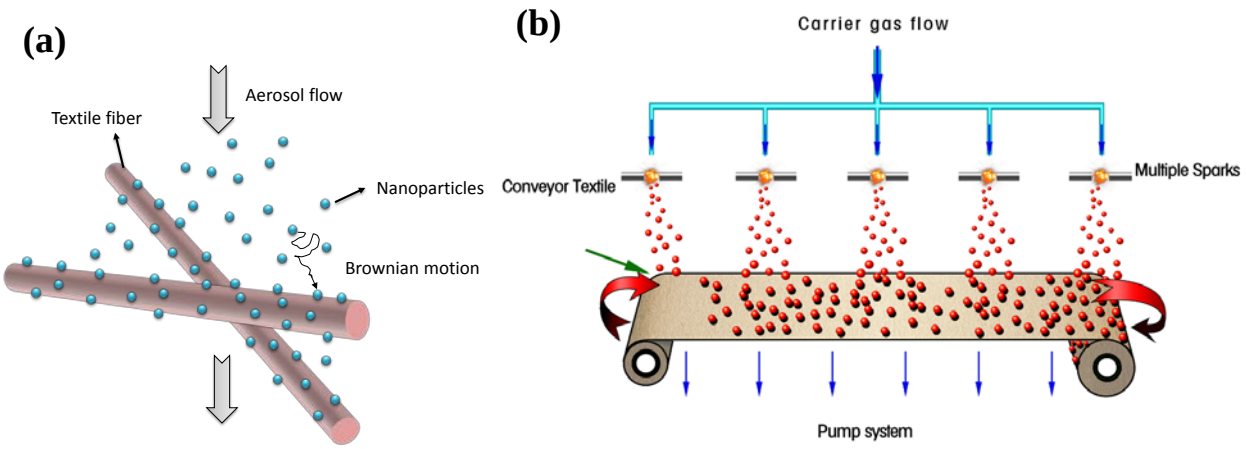

Figure 1. Illustration of the fabrication process. (a) An aerosol flow is passed through the textile, where the NPs collide and stick to the fibers by van der Waals forces. The NP-fiber collision is caused by the NP Brownian motion. (b) Conceptual design of a simple, scalable and green route for textile nanofinishing achieved by integrating electrical discharges for the synthesis of NPs into roll-to-roll textile production**.**

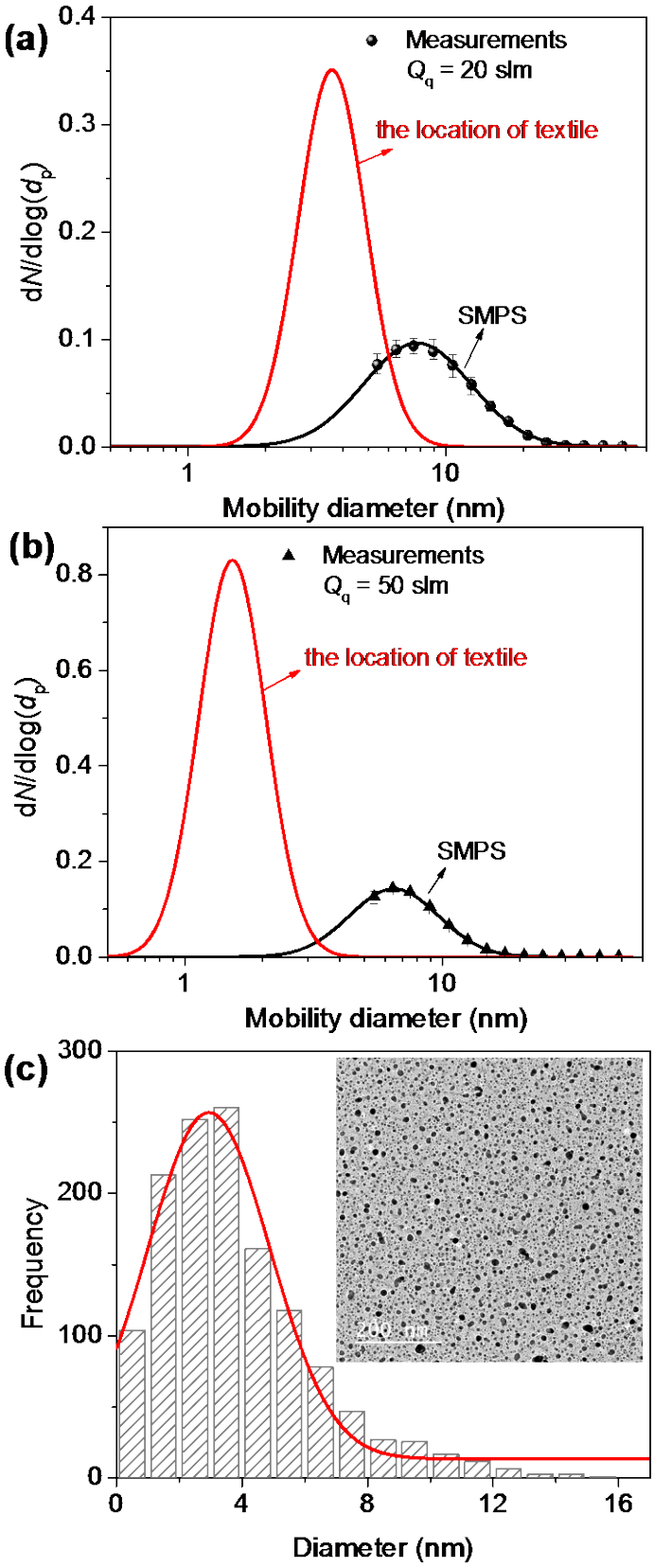
(a)
Measurements
Q_q = 20 slm
the location of textile
SMPS
dN/dlog(d_p)
Mobility diameter (nm)
(b)
Measurements
Q_q = 50 slm
the location of textile
SMPS
dN/dlog(d_p)
Mobility diameter (nm)
(c)
Frequency
Diameter (nm)

Figure 2. Particle Size distributions at quenching gas flow rates of (a) Q_q = 20 slm; (b) Q_q = 50 slm. The black **s**ymbols and curves correspond to the particle size distributions measured directly by the SMPS and to the fitted lognormal distributions, respectively, while the red curves correspond to the particle size distribution at the location of the textiles as estimated by considering the growth of the particles along the sampling line to the SMPS. **c**, the particle size distribution is based on the TEM image (Q_q = 20 slm).

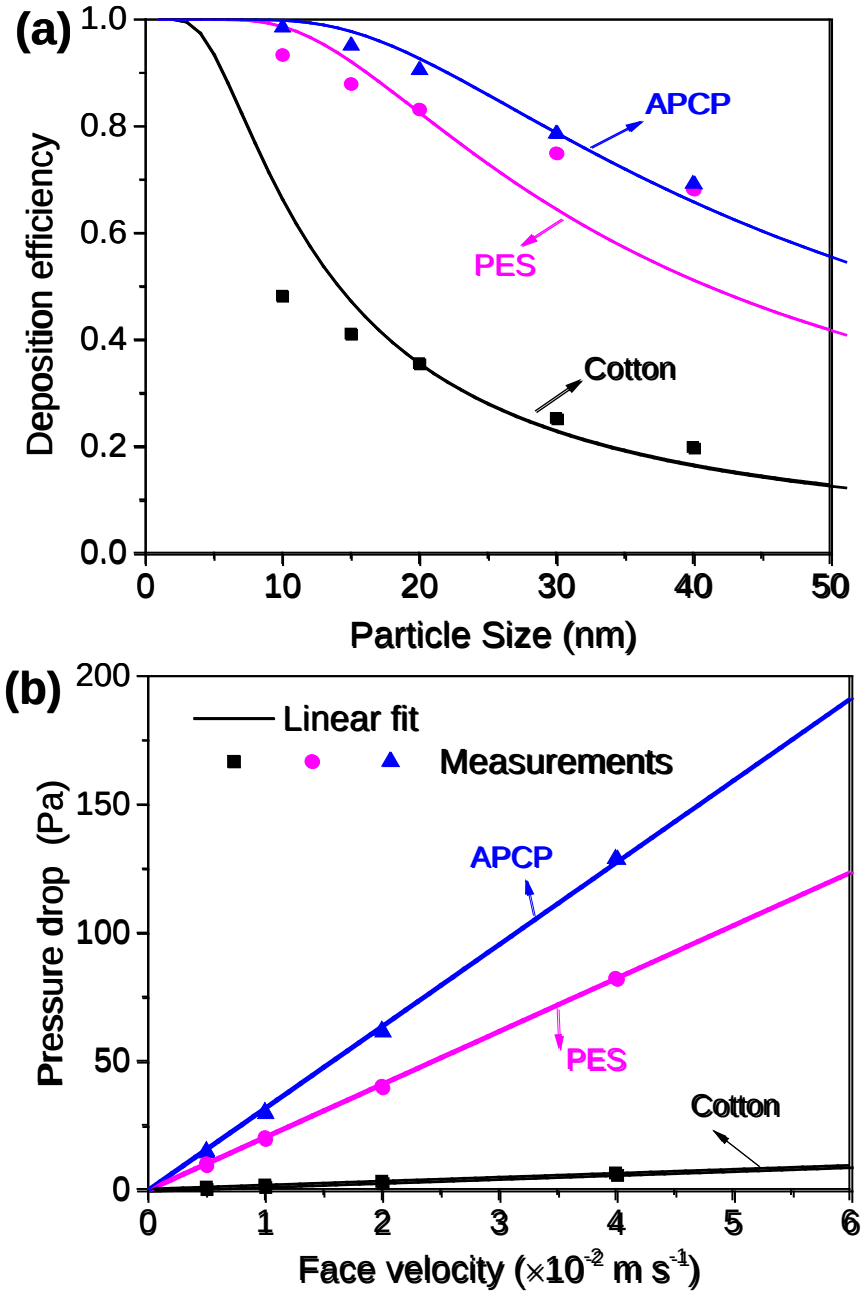

Figure 3. Variation in filtration performance of the textiles. (a) deposition efficiency as a function of particle diameter for a face velocity of 0.02 m s^{-1}. The curves represent predictions using equation (1), whereas the symbols correspond to the deposition measurements. (b) flow pressure drop across the textiles as a function of face velocity.

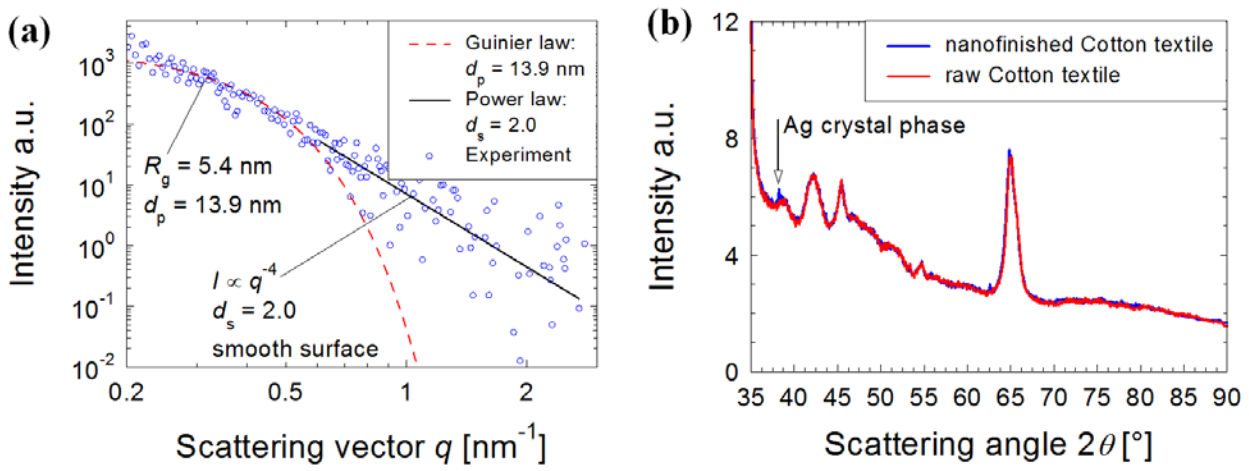

Figure 4. SAXS/WAXS data for Cotton textile. (a) SAXS data for Cotton textiles treated with Ag NPs. (b) the WAXS patterns seen in raw and nanofinished Cotton.

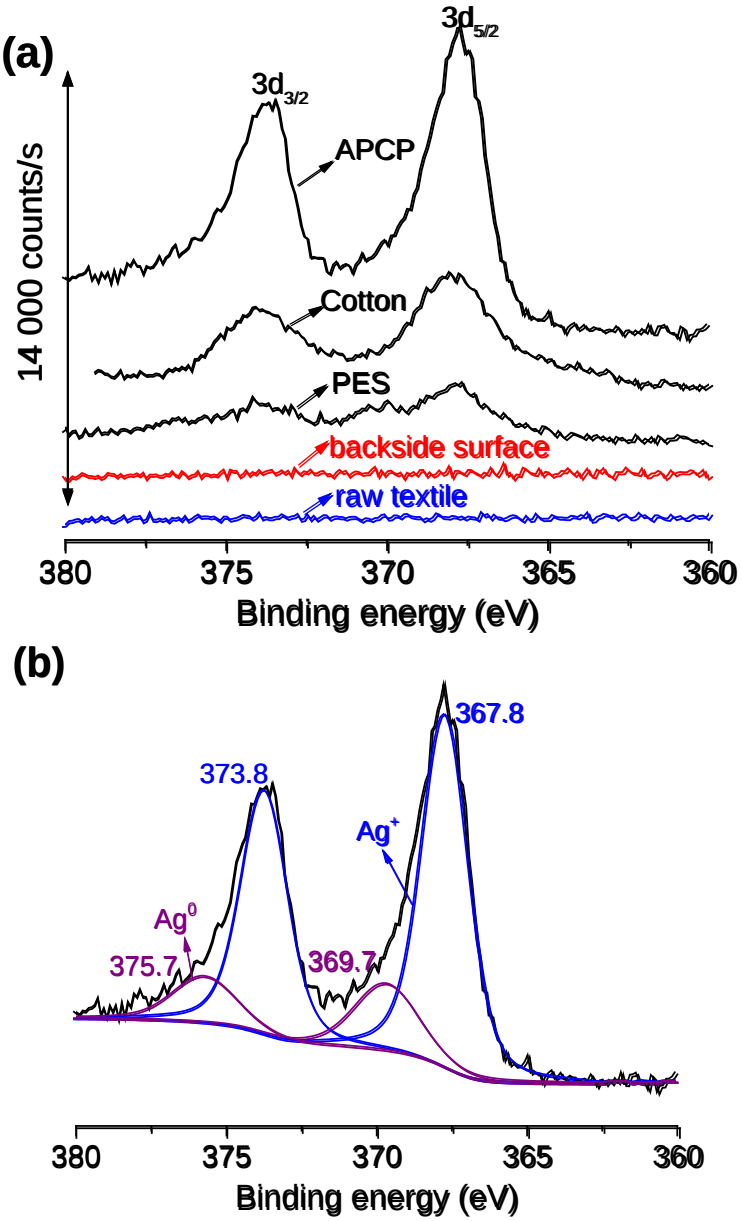

Figure 5. Compositional characterization of Ag NPs deposited on textiles. (a) High-resolution Ag 3d ($3d_{5/2}$ and $3d_{3/2}$) XPS region spectra of APCP, Cotton, and PES textiles, including the front side surface (black curves) and the backside surface (red line) of the nanofinished fabrics, and the surface of the raw textiles (blue line). As all the three raw textiles and their backsides have flat lines, the red and blue lines are valid for all these three textiles. The total intensity of the two peaks reflects the different contents of Ag on the nanofinished textiles, in line with the ICP-MS measurements (Table S3). (b) the deconvolution of the Ag 3d peaks for the nanofinished APCP textile.

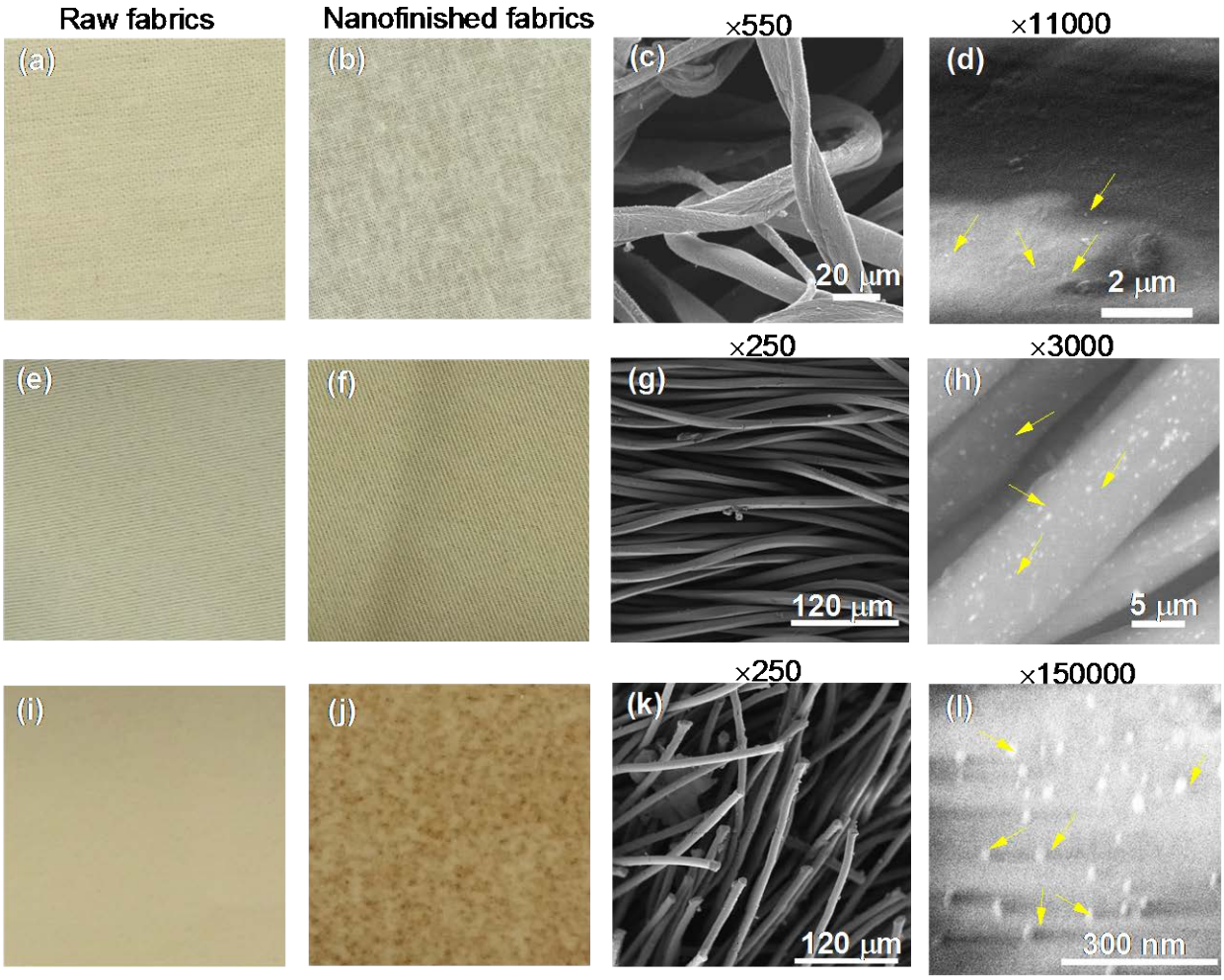

Figure 6. Optical change of the fabrics before and after the deposition of Ag NPs (two left columns) and SEM images of the nanofinished textiles (two right columns). (a-d) Images of raw and nanofinished Cotton fabrics, together with two sets of SEM images with ×550 (acceleration voltage at 5 kV) and ×11000 (acceleration voltage at 3 kV) magnification. (e-h) Images of raw and nanofinished PES fabrics, together with two sets of SEM images with ×250 (acceleration voltage at 5 kV) and ×3000 (acceleration voltage at 3 kV) magnification. (i-l) Images of raw and nanofinished APCP fabrics, together with two sets of SEM images with ×250 (acceleration voltage at 5 kV) and ×150000 (acceleration voltage at 3 kV) magnification.

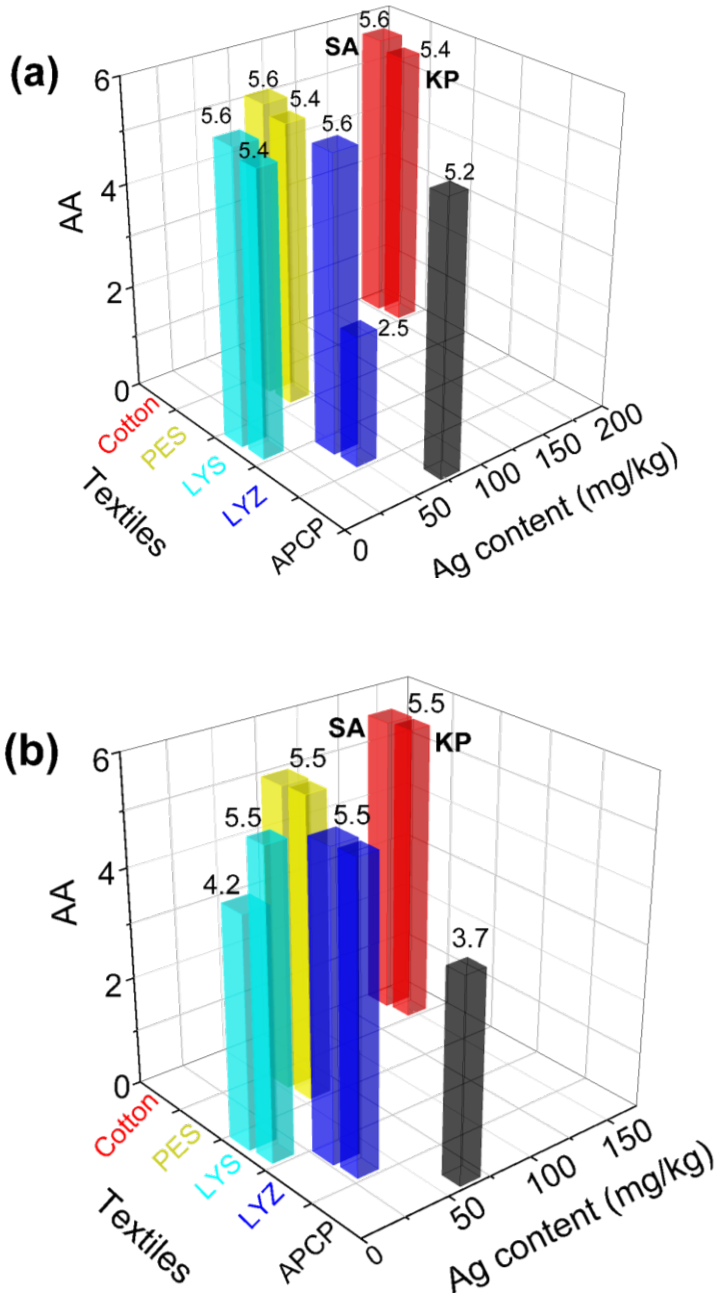

Figure 7. Antibacterial activity (AA) of the textiles treated with Ag NPs against *Staphylococcus Aureus* (SA), and *Klebsiella Pneumoniae* (KP), as shown respectively in the left and right rectangular columns of the same textile. (a) antibacterial activity of non-washed textiles versus Ag content; (b) antibacterial activity of washed textiles (three cycles, only five cycles for APCP) versus Ag content.

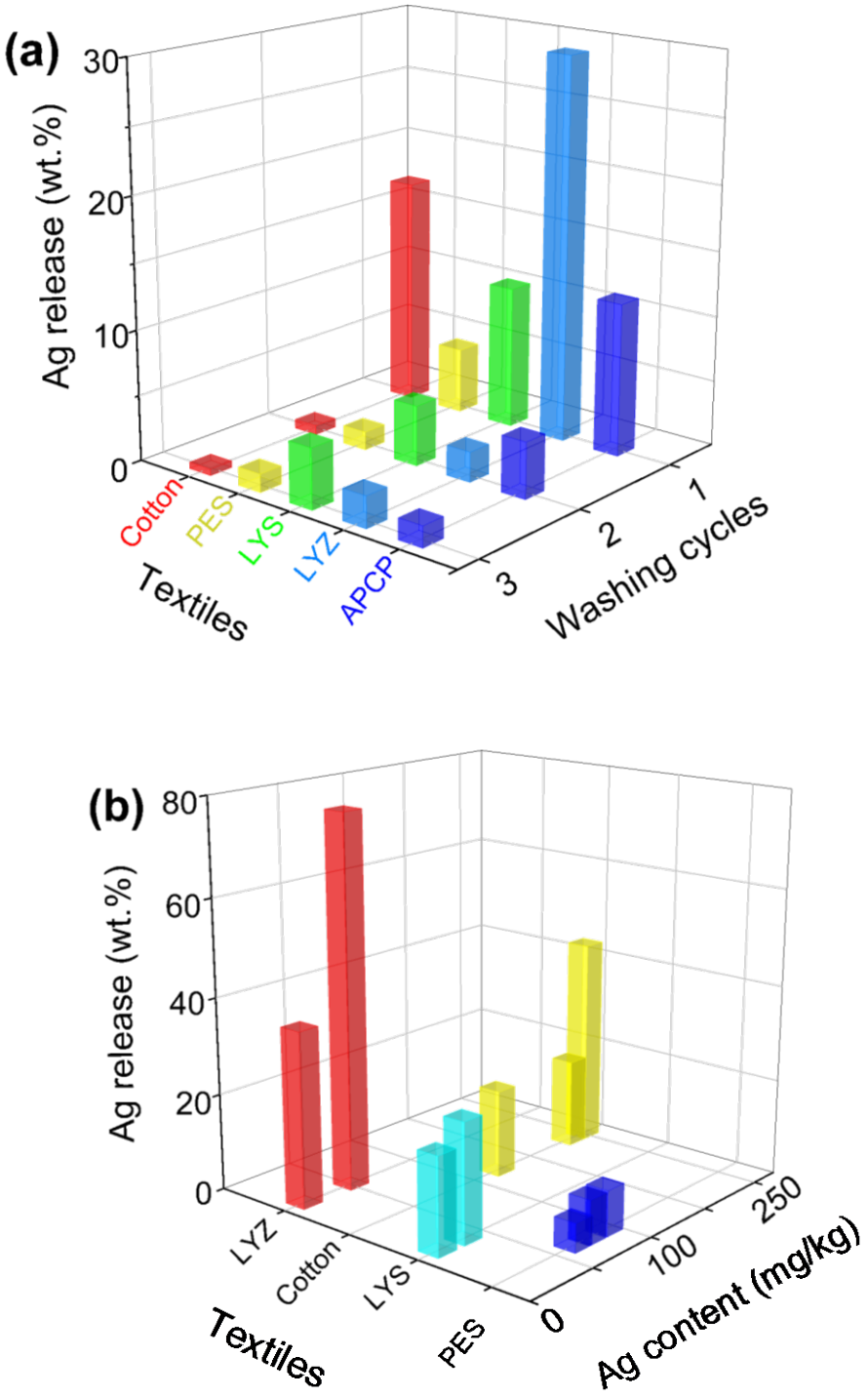

Figure 8. Ag NP release from the nanofinished textiles as a function of (a) washing cycles and (b) Ag content.

TOC

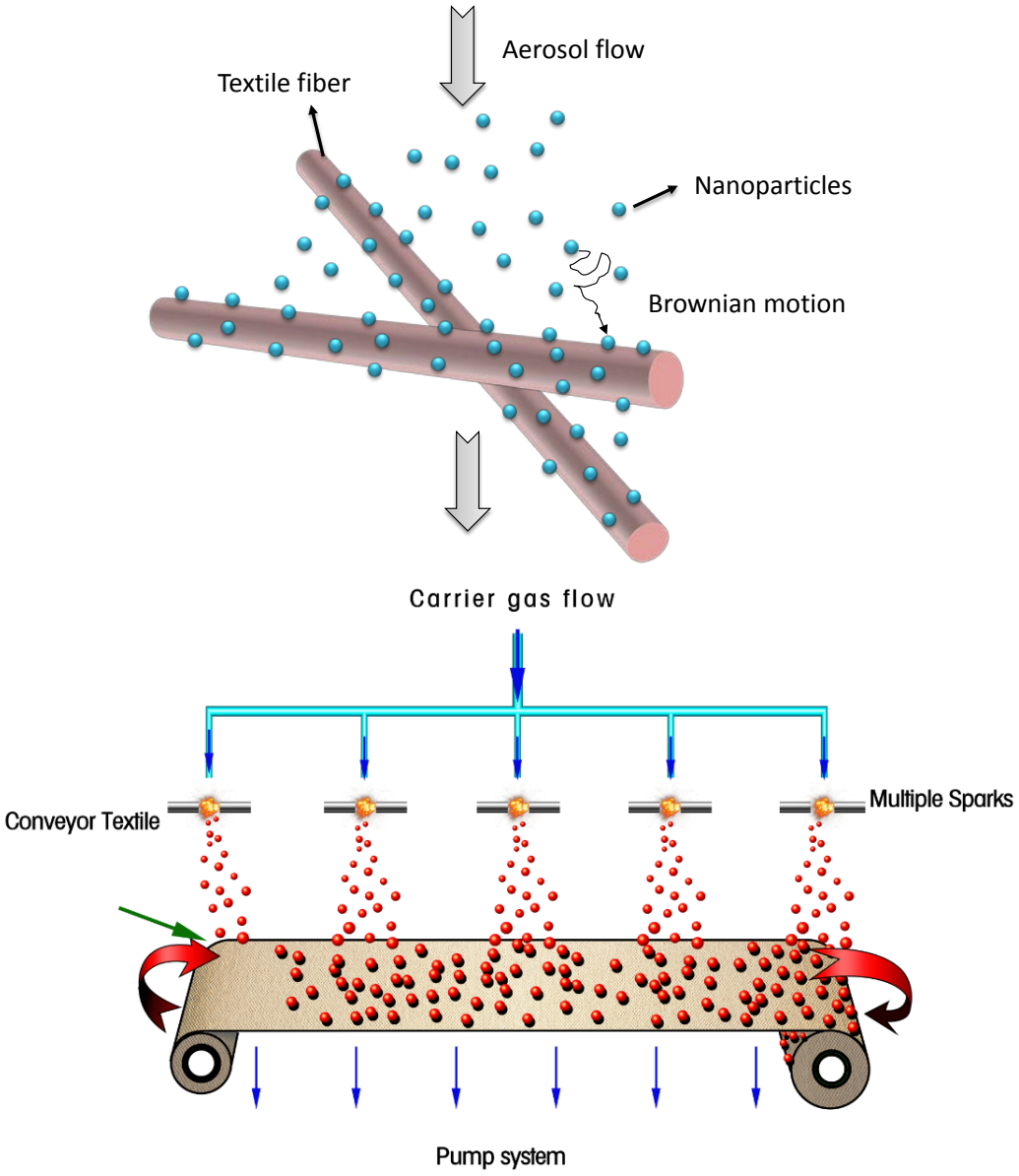
Aerosol flow
Textile fiber
Nanoparticles
Brownian motion
Carrier gas flow
Conveyor Textile
Multiple Sparks
Pump system